Wang, Xuchen; Asadchy, Viktar S.; Fan, Shanhui; Tretyakov, Sergei A.

Space-Time Metasurfaces for Power Combining of Waves

Published in:
ACS Photonics

DOI:
10.1021/acsphotonics.1c00981

Published: 20/10/2021

Document Version
Publisher's PDF, also known as Version of record

ACS Photonics

pubs.acs.org/journal/apchd5

Article

Space–Time Metasurfaces for Power Combining of Waves

Xuchen Wang,* Viktar S. Asadchy, Shanhui Fan, and Sergei A. Tretyakov

Cite This: *ACS Photonics* 2021, 8, 3034–3041

Read Online

ACCESS | Metrics & More | Article Recommendations | Supporting Information

ABSTRACT: In passive, linear, and monochromatic systems, complete and phase-insensitive combining of powers carried by waves from several input channels into a single output channel is forbidden by the energy conservation law. Here, we demonstrate that the complete combination of both coherent and incoherent plane waves can be achieved using metasurfaces with properties varying in space and time. The proposed structure reflects waves of the same frequency but incident at different angles toward a single direction. The frequencies of the output waves are shifted by the metasurface, ensuring perfect incoherent power combining. The proposed concept of power combining is general and can be applied for electromagnetic waves from the microwave to optical domains, as well as for waves of other physical natures.

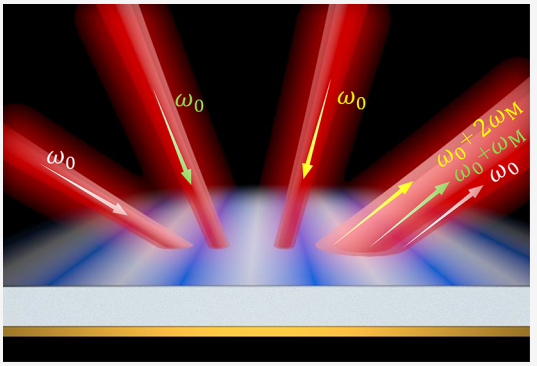

KEYWORDS: *beam combination, incoherent excitation, Floquet theorem, high-power sources, photon flux, frequency conversion, time-varying materials*

Combining electromagnetic waves from multiple input ports into a single output port is highly desired in optical and microwave engineering. It would overcome power limits of conventional sources, enabling high-power laser and long-distance free-space communications. The most straightforward approach for wave combining is based on beam splitters or power dividers.[1] However, these passive components allow complete combination of coherent beams only when the beams have specific phase and amplitude relations among them. This constraint originates from the passivity of the system.[2,3] In general, input ports of a passive combiner are not matched, and, when excited by incident waves, parasitic reflections appear. Only when the combiner is coherently illuminated from all the input ports simultaneously, with specific phases of each input wave, the reflections will interfere destructively, and all the input power can be directed to the output port. Such a phase- and amplitude-sensitive operation is analogous to that of recently proposed coherent absorbers and lasers.[4] However, in most practical scenarios, incident coherent waves have arbitrary phases and amplitudes, and, therefore, the condition of destructive interference of parasitic reflections is not satisfied, and the combining efficiency drops significantly.

For incoherent incident waves, the passivity constraint does not hold since the waves do not interfere, and the combined output intensity is merely a sum of the input intensities. This opportunity has been widely used in high-power lasers and electromagnetic waves. It is, for example, certainly possible to combine the power of two waves with orthogonal polarizations, but in this case, the number of incoming waves is limited to two.[5] One can also combine waves with different frequencies, which is also known as wavelength beam combining. Using dispersive elements (prisms or gratings), beams from different directions propagating at different frequencies can be collimated at the same output direction.[6−8] For example, using one[9,10] or a pair of grating structures,[8] the beams from an incoherent laser array are overlapped in one direction through materials with normal dispersion. Nevertheless, the emission wavelengths from each source must be accurately controlled. In addition, this method cannot be used to combine low-terahertz and microwave beams with small frequency differences Δf because the required size of gratings would be enormous due to scaling as $1/\Delta f$.[7,11] Therefore, it is highly desirable to have a compact system to efficiently combine powers from different ports without restrictions on amplitudes, phases, and frequency differences for the input beams.

An alternative way to avoid the passivity condition is to modulate the system dynamically in time. In recent years, time-modulated structures have shown great possibilities to achieve exotic wave effects, i.e., unlimited energy accumulation,[12] temporal Wood anomalies effect,[13] and so on. Within this framework, spatiotemporal metasurfaces recently demonstrated great potential for a plethora of applications, such as Doppler-type frequency shift,[14] isolation,[15−17] circulation,[18]

Received: July 1, 2021
Published: September 21, 2021

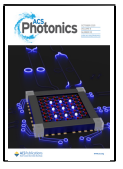

nonreciprocal phase shifting,[15] and beam splitting.[19] In this paper, we use reflective space−time modulated metasurfaces to realize perfect power combining for both coherent and incoherent plane waves. We show that such metasurfaces can provide complete power combining in reflection for waves incident from several predefined directions having identical frequencies but arbitrary phases and amplitudes. The spatial modulation in the metasurface ensures that all the incident waves are reflected into a single output channel. Because of the temporal modulation, incident same-frequency plane waves are reflected as waves with slightly different frequencies, allowing perfect incoherent power combining in the output channel. We provide several metasurface designs for complete power combining with weak frequency conversion (using slow temporal modulations). In all the cases, the combined power at the output channel can be captured by a single receiver with finite bandwidth.

RESULTS AND DISCUSSION

In what follows, we describe periodic metasurfaces as multiport systems characterized by scattering matrix $\overline{\overline{S}}$.[20] Propagating Floquet harmonics for a given illumination direction represent orthogonal channels and are equivalent to physical ports of a multiport system.

First, we show that linear time-invariant systems (both passive and active) cannot provide complete power combining for coherent plane waves with arbitrary phases and amplitudes. To keep the discussion general, we consider a multiport system shown in Figure 1, which can describe power combining in

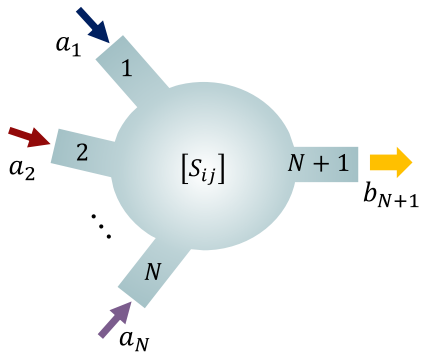

Figure 1. A general time-invariant power combiner with N input ports and one output $(N + 1)$st port.

various scenarios: metasurfaces, electrical networks, waveguides, etc. The multiport system is excited at input ports i $(1 \le i \le N)$ with some field amplitudes $a_i = A_i e^{j\phi_i}$, where ϕ_i are real and A_i are positive real quantities. The output port $N + 1$ is not excited; that is, $a_{N+1} = 0$. From the scattering matrix of the system $\overline{\overline{S}}$, we can find the output field at this port as $b_{N+1} = \sum_{i=1}^{N} S_{N+1,i} a_i$. The efficiency of power combining expressed as the ratio of the output power in port $N + 1$ to the total input power at ports from 1 to N reads

$$\eta(a_i) = \frac{\left|\sum_{i=1}^{N} S_{N+1,i} A_i e^{j\phi_i}\right|^2}{\sum_{i=1}^{N} A_i^2} \tag{1}$$

As seen from eq 1, the combining efficiency strongly depends on the amplitudes and phases of the input fields, for both passive and active systems. For any S-matrix, there in fact exist input fields for which the power-combining efficiency is exactly zero. For arbitrary input fields a_i, the efficiency is always limited by (see section 1 of the Supporting Information)

$$\eta(a_i) \le \sum_{i=1}^{N} |S_{N+1,i}|^2 \tag{2}$$

In active systems, the combining efficiency can be larger than unity for some input fields a_i. On the other hand, in passive systems, the efficiency obeys $\eta(a_i) \le 1$. The inequality becomes equality only if the following three conditions hold: (i) port $N + 1$ is matched; that is, $S_{N+1,N+1} = 0$; (ii) there is no energy dissipation in the system; (iii) all the input fields satisfy the same condition $a_i = CS^*_{N+1,i}$, where C is a complex constant and "*" denotes a complex conjugate.

In the special case when a passive multiport network is excited only at one port i $(1 \le i \le N)$, one can calculate the average efficiency (averaged over all N ports) of power coupling into the output port $N + 1$ as (see section 2 of the Supporting Information)

$$\eta_{\text{coupl}} = \frac{1}{N}\sum_{i=1}^{N} |S_{N+1,i}|^2 \le \frac{1}{N} \tag{3}$$

The average efficiency of power combining can reach its maximum value $\eta_{\text{coupl}} = 1/N$ only in the absence of power dissipation and if the output port is matched. We see that with increasing the number of input ports N, the average coupling efficiency linearly decreases. Furthermore, complete power combining from multiple input ports becomes exceedingly difficult with increasing N due to the requirement of mutual coherence of the incident waves. Obviously, the phase-dependent operation is not desired in practical applications of power combining. In linear time-invariant systems, the problem cannot be avoided because the monochromatic outgoing waves at the output port always interfere.

In order to overcome these fundamental constraints on power combining, we propose to exploit a metasurface possessing both spatial and temporal modulations of its electromagnetic properties. Such a time-varying multiport system introduces a frequency shift between the output waves making them incoherent. Because of this incoherence, the device can fully combine waves *of the same frequency* from multiple input ports to a single output port and operate efficiently for both single and multiport input waves with arbitrary amplitudes and phases. The operational principle of the metasurface is illustrated in Figure 2. Plane waves of the same-frequency ω_0 incident at different angles on the metasurface (illustrated by three separate scenarios) are completely reflected to the same direction, at an angle θ_r. The temporal modulation of the metasurface adds different frequencies (temporal momenta) to the three reflected waves: 0, $\Delta\omega_2$, and $\Delta\omega_3$, respectively. Therefore, the output waves in all the scenarios become incoherent (for coherent inputs), and their powers can be perfectly combined. The identical reflection angles for the output waves are ensured by proper spatial modulation of the metasurface: the reflected waves gain different spatial momenta, 0, $\Delta\mathbf{k}_2$, $\Delta\mathbf{k}_3$, respectively, such that they are deflected toward the same direction. We model the metasurface as an impedance sheet positioned on a grounded dielectric substrate, as shown in Figure 3. Such geometry was previously exploited both for time-invariant[21] and time-varying[16,22,23] metasurfaces. Here, we model the impedance

https://doi.org/10.1021/acsphotonics.1c00981
ACS Photonics 2021, 8, 3034−3041

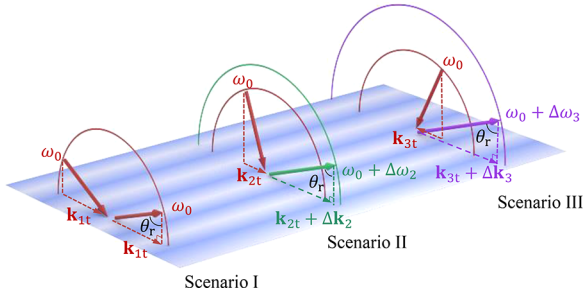

Figure 2. Principle of complete power combining using space−time metasurfaces. The metasurface totally reflects incident plane waves coming from three different directions (three scenarios) into the same output direction at an angle θ_r. The metasurface imparts both tangential spatial and temporal momenta onto incident waves, modifying the isofrequency curves.

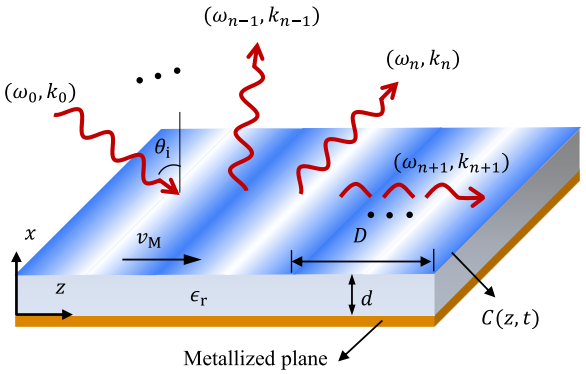

Figure 3. Scattering from a space−time modulated impedance sheet positioned on a grounded substrate.

sheet as a spatiotemporally modulated sheet capacitance $C(z, t)$. Such an impedance sheet can be realized at microwave frequencies by a metallic pattern with embedded varactors (voltage-controlled capacitors). For optical frequencies, temporal modulations of this type can be realized using voltage-biased *pn*-junction electrical diodes[24] or a nonlinear Kerr effect.[25]

The modulation of surface capacitance has a traveling waveform with spatial period D (along the z-direction) and temporal period T, and therefore the modulation velocity is $v_M = D/T$. Because of the periodicity, the modulation function can be expanded into the Fourier series

$$C(z, t) = \sum_{m=-\infty}^{+\infty} c_m e^{-jm(\beta_M z - \omega_M t)} \tag{4}$$

where $\beta_M = 2\pi/D$ and $\omega_M = 2\pi/T$ are the spatial and temporal modulation frequencies, respectively, and $c_m = c_{-m}^*$ to ensure $C(z, t)$ is real function.

We consider a transverse electric (TE) plane wave incident from $\theta = \theta_i$ at a frequency ω_0. The incident wavenumber in free space is denoted as k_0. Because of the spatial modulation, the incident wave is scattered into infinitely many spatial harmonics with tangential wavenumbers $k_{zn} = k_0 \sin\theta_i + n\beta_M$, and due to the time modulation, the propagation frequency of wave in the nth spatial channel is $\omega_n = \omega_0 + n\omega_M$.[15] The wavevector of the nth harmonic must respect the dispersion relation in free space, $k_n = |\omega_n|\sqrt{\epsilon_0\mu_0}$. If $|k_{zn}| < |k_n|$, the harmonic is propagating wave and scattered into free space. If $|k_{zn}| > |k_n|$, the harmonic is evanescent. Once the spatial and temporal modulation periods, the frequency of the incident waves, and the incidence directions are known, the directions of scattering channels (free-space propagating modes) can be determined according to the Floquet theorem. When the capacitance function $C(z, t)$ and the substrate properties (permittivity ε_r and thickness d) are chosen, we calculate the amplitudes and phases of all the scattering harmonics. Several theoretical methods have been proposed to calculate scattering by space−time varying metasurfaces, e.g., Floquet mode-matching method[15] and boundary matching based on dynamical differential formalism.[26] Here, we choose mode-matching methods (see section 3 of the Supporting Information).

The schematics of a general multiport metasurface combiner is depicted in Figure 4, where ports from 1 to N are the input

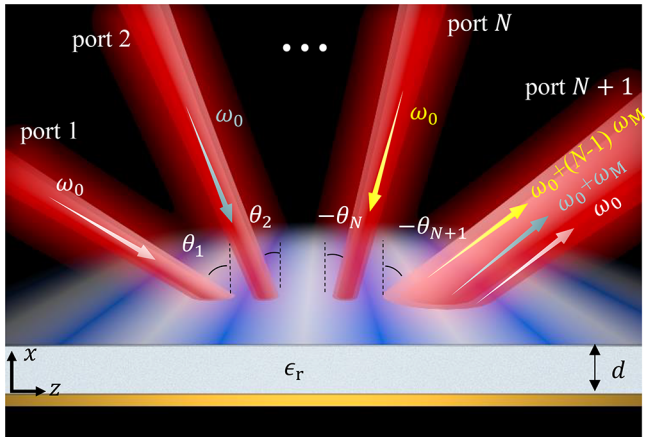

Figure 4. Schematics of a general $N + 1$ metasurface power combiner. The output port is along the specular direction of incidence from port 1, i.e., $\theta_1 = \theta_{N+1}$. All the angles are counted from the metasurface normal in the anticlockwise direction.

ports, and port $N + 1$ is the output port. The directions of the input ports are denoted by the incident angles θ_n, where $n \in [1, N]$ represents the input port index. The output port is along the specular direction of port 1. Thus, when illuminated from port 1, the reflection to port $N + 1$ corresponds to the zero-order harmonic of the metasurface. Consecutively, a wave incident from port n ($n \in [1, N]$) is reflected to port $N + 1$ as the $(n - 1)$th Floquet harmonic. According to the Floquet−Bloch theorem, the tangential wavevectors of incidence and its $n - 1$ reflection mode are related by the expression

$$k_0 \sin\theta_n + (n - 1)\beta_M = \alpha_n k_0 \sin\theta_1 \tag{5}$$

where $\alpha_n = \left|\frac{\omega_0 + (n-1)\omega_M}{\omega_0}\right|$. Next, we specify the incidence angles of port 1 and port N (denoted as θ_1 and θ_N), and thus the spatial period can be determined from eq 5:

$$D = \frac{(N - 1)\lambda_0}{\alpha_N \sin\theta_1 - \sin\theta_N} \tag{6}$$

By substituting eq 6 into eq 5, one can uniquely determine the angles of port n for $n \in [2, N - 1]$:

$$\sin\theta_n = \alpha_n \sin\theta_1 - \frac{(n - 1)(\alpha_N \sin\theta_1 - \sin\theta_N)}{N - 1} \tag{7}$$

https://doi.org/10.1021/acsphotonics.1c00981
ACS Photonics 2021, 8, 3034−3041

As soon as the spatial period, modulation frequency, and the directions of all ports are fixed, one can optimize the space−time modulation profile and achieve full reflection from all input ports to the output port $N + 1$.

According to the Manley−Rowe relations,[27] while the energy in time-varying systems is not conserved, the total number of photons entering a lossless system must be equal to that leaving the system. Since our metasurface does not include energy-dissipating components, it will conserve the photon flux. Because of the periodicity and infinite extent of the metasurface, the *normal* components of the total incident photon flux per unit area $P_{i,x}/(\hbar\omega_i)$ and that of the total reflected photon flux $P_{r,x}/(\hbar\omega_r)$ must be equal for any illumination. Here, P_x denotes the normal component of the Poynting vector, and it is proportional to $E_i^2 \cos\theta_i$ for incident and to $E_r^2 \cos\theta_r$ for reflected plane waves. To achieve complete power combining using the metasurface, it is sufficient to ensure that, when illuminated from a single port n ($n \in [1, N]$), the metasurface will reflect all the photons into port $N + 1$. Therefore, we optimize the metasurface so that for single-port excitation the following relation approximately holds:

$$E_{r,N+1} = \sqrt{\frac{\omega_r}{\omega_i}\frac{\cos\theta_n}{\cos\theta_{N+1}}}\,E_{i,n} \tag{8}$$

Here, $\omega_i = \omega_0$ is the frequency at the input port n and $\omega_r = \alpha_n\omega_0$ is the frequency at the output port $N + 1$. For illumination from multiple ports ($n \in [1, N]$), all the photons will be automatically reflected into port $N + 1$ if (8) holds, due to the incoherence of the output waves.

To satisfy (8) for ports $n \in [1, N]$, we employ numerical tools to optimize the metasurface parameters. There are in total N optimization objectives for a metasurface with a given substrate thickness and substrate permittivity. We use the "fmincon" function in MATLAB for optimizing the Fourier coefficients of the modulation function c_m of the metasurface, as we show in the Supporting Information. The reflected fields are calculated using the mode-matching method (see section 3 of the Supporting Information). It should be noted that for one specific incidence, the summation of near- and far-field scattering modes should satisfy the boundary condition. Therefore, the same scattered far fields can be created by different impedance boundaries which support different sets of evanescent modes. This feature indicates that one can find multiple solutions for modulation functions that fulfill our objectives for scattered far fields.

Next, to demonstrate the universality of the proposed concept based on an example, we design a three-port ($N = 2$) metasurface power combiner. Without loss of generality, we specify the angles of ports 1 and 2 as $\theta_1 = +45°$ and $\theta_2 = 0°$, respectively. The output port 3 is at the angle $\theta_3 = -\theta_1 = -45°$ (all the angles are counted from the metasurface normal in the anticlockwise direction, as shown in Figure 4). The incident frequency is ω_0, and the modulation frequency is assumed to be much smaller than the incident frequency (as an example, we select $\omega_M = 0.05\omega_0$), such that only ports 1, 2, and 3 support propagating waves in free space, and other higher-order harmonics excited at the metasurface are evanescent. The advantage of the slow modulation scenario is that such a metasurface can be relatively simply implemented.[16,22,24,25,28−30] Moreover, the converted frequencies at the output port only slightly differ from the incident frequency so that all power can be efficiently received even by a receiver with a small bandwidth. On the basis of these parameters, the spatial modulation period is determined from eq 6 as $D = 1.346\lambda_0$. The substrate thickness is $d = 8.7 \times 10^{-3}\lambda_0$, and $\epsilon_r = 3$. To find the proper modulation function of the capacitive impedance sheet that can realize full photon delivery from ports 1 and 2 to port 3, two optimization objectives are set in numerical optimization according to eq 8. The first one ensures full specular reflection from port 1 to port 3; i.e., $E_{r,3} = E_{i,1}$. The second objective is $E_{r,3} \approx 1.219E_{i,2}$, which ensures full anomalous reflection from port 2 to port 3. Since the number of objectives is two, in principle, we need to introduce more than two degrees of freedom (Fourier terms in the modulation function). Here, we optimize four Fourier coefficients, namely, c_0, $c_{\pm1}$, $c_{\pm2}$, and $c_{\pm3}$. One of the optimized solutions is

$$\begin{aligned} C(z, t) = 0.062[1 &- 0.152\cos(\beta_M z - \omega_M t) - \\ &0.01\cos(2\beta_M z - 2\omega_M t - 0.26\pi) - \\ &0.02\cos(3\beta_M z - 3\omega_M t - 0.97\pi)]\cdot\omega_0^{-1}[F] \end{aligned} \tag{9}$$

Note that this modulation function is independent from the relative phases of waves input to different ports. As soon as the modulation function is obtained, the amplitudes of all the scattering harmonics for each incidence can be calculated following the mode-matching method.

Figure 5 shows the scattering harmonics for two illumination scenarios: from port 1 and from port 2. One can see that the two objectives defined in the optimization are reached with negligible errors, and undesired waves scattered into input ports have negligible amplitudes. In addition to the realized power combining of propagating modes, strong evanescent modes (shown by dashed lines) are excited at the metasurface, but they do not carry power in the normal direction. Nevertheless, the excitation of evanescent modes is essential

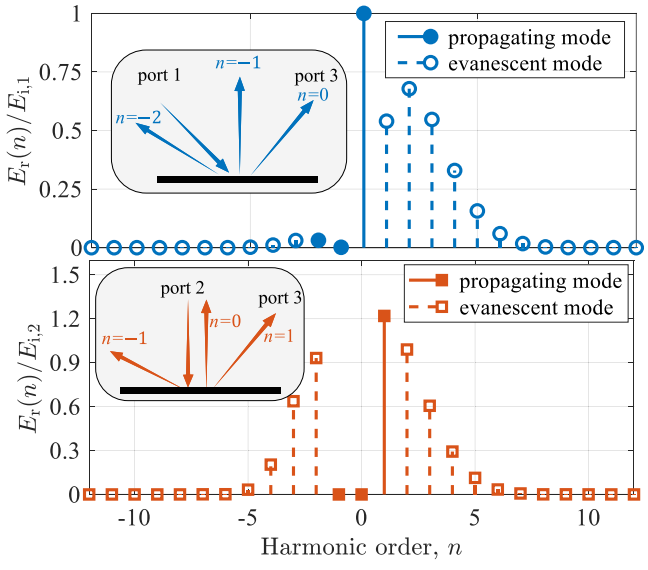

Figure 5. Normalized amplitudes of scattering harmonics for illuminations from port 1 (top) and port 2 (bottom). Here, index n inside the brackets denotes the scattered harmonic orders that correspond to different ports in the top and bottom subpanels, as depicted in the insets. The scattering harmonics of higher orders are negligibly small.

https://doi.org/10.1021/acsphotonics.1c00981
ACS Photonics 2021, 8, 3034−3041

to satisfy the boundary conditions that simultaneously ensure desired scattering for both illumination scenarios.

Knowing the amplitudes of all the scattering harmonics, the photon flux reflectance (the ratio of the normal components of the reflected and incident photon fluxes per unit area) at each port can be calculated as $R = E_r^2 \cos\theta_r\omega_i/(E_i^2 \cos\theta_i\omega_r)$. Table 1 shows the calculated values. As is seen, almost all the incident photons are reflected to port 3 for illuminations from ports 1 and 2. For completeness, the last column of the table presents the results for the case when the metasurface is illuminated at port 3. The total number of photons is conserved for each illumination scenario (the sum of reflectances in each table column equals unity), as expected for a lossless time-modulated metasurface. Generally speaking, the designed metasurface can be described by a normalized scattering matrix whose entries relate the input and output tangential electric fields normalized by the square roots of the corresponding frequencies.[31] Since the metasurface is lossless, this scattering matrix is unitary. Since the metasurface exhibits both spatial and temporal modulations, the scattering matrix has an infinite number of elements. The truncated matrix for the designed metasurface can be found in section 4 of the Supporting Information.

Table 1. Photon Flux Reflectances from the Metasurface Modulated at $\omega_M = 0.05\omega_0$[a]

illumination from port 1	illumination from port 2	illumination from port 3
R_{11} = 0.079%	R_{12} = 0.000%	R_{13} = 9.025%
R_{21} = 0.000%	R_{22} = 0.000%	R_{23} = 73.159%
R_{31} = 99.921%	R_{32} = 100.000%	R_{33} = 17.816%

[a] R_{pq} is the reflectance for incidence from port q to port p.

An important characteristic of a power-combining device is its bandwidth. Figure 6 shows the reflection efficiencies from ports 1 and 2 to port 3, when the incident frequency is swept around ω_0. At the operating frequency $\omega = \omega_0$, the reflection reaches the maximal value for both R_{31} and R_{32}. This is what we have targeted in the optimization. At the frequency of $\omega = 0.964\omega_0$, specular reflectance R_{31} reaches almost zero because at this frequency the space–time metasurface operates as a retroreflector. Moreover, there exists a minimum for R_{32} at the frequency of $\omega = 1.033\omega_0$, where photons from port 2 are reflected anomalously to port 1 and specularly back to port 2. From Figure 6, one can estimate the relative bandwidth of the metasurface to be in the range of 2%. Increasing the modulation depth can widen the bandwidth of the metasurface.[17,32] The moderate bandwidth of the metasurface implies that it can be designed also for combining pulses, providing that their spectra are within the metasurface bandwidth. It should be noted that when the incident frequency changes, the direction of port 2 also changes according to eq 6 because the modulation parameters (D and ω_M) and angle θ_1 are assumed to be constant. Thus, for excitations in the form of pulses, different frequency components of the second pulse (impinging from port 2) must have different oblique angles $\theta_2(\omega)$. Such spatial dispersion of the incident pulse can be generated using conventional techniques with additional diffraction elements.[33] Figure 7 presents a possible schematic of a metasurface for pulse combination. A diffraction grating is used to generate a properly diverged incident pulse at port 2 so that it compensates for the spatial dispersion of the metasurface. As a result, all the frequency components of the pulse are reflected to the same output direction.

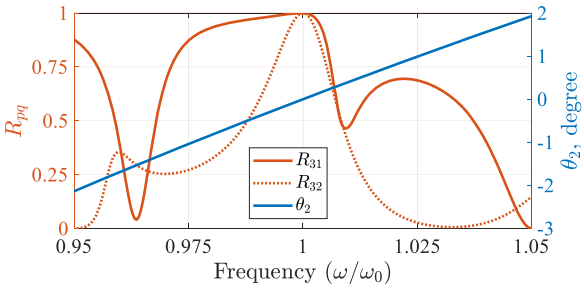

Figure 6. Left axes: photon flux reflectance from ports 1 and 2 to port 3. Right axes: variation of the angle of the port 2 direction as the incident frequency changes.

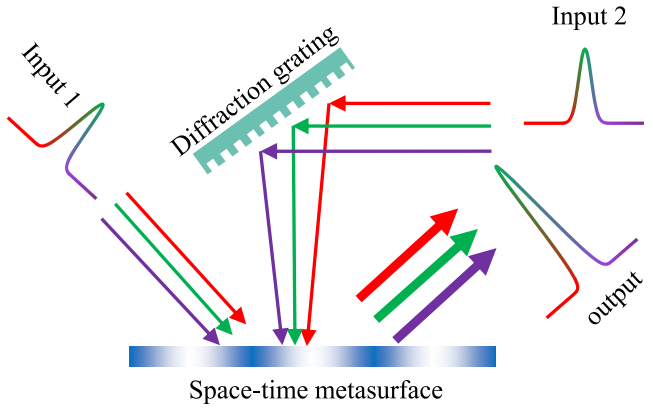

Figure 7. Possible implementation schematics for power combination of pulses using space–time metasurfaces. According to the blue line in Figure 6, the low-frequency (denoted with red arrows) and high-frequency (denoted with purple arrows) components of the pulse impinge on the metasurface at the negative and positive incident angles, respectively.

The above results show power combining from two input ports. The proposed method can be generalized to design power concentrators with an arbitrary number of input ports. As the number of ports increases, the number of objectives in optimization also increases, and one needs to introduce more Fourier terms in the modulation function. Alternatively, one can introduce additional reactive components in the surface impedance to increase the design freedom. Section 5 of the Supporting Information includes a design of a four-port power-combining metasurface.

In order to address potential implementations of a power combiner metasurface based on the proposed principle, next we analyze how the modulation depth (modulation amplitude) of the capacitance affects the device performance. Such an analysis is essential since in most practical scenarios the attainable modulation depth is limited, especially at higher frequencies.[32] As it was shown in ref 17, for many devices the modulation depth of time-varying metasurfaces is not a critical parameter, and good performance can be obtained even for small values of this parameter at the expense of increased quality factor (decreased operational bandwidth). Figure 8 demonstrates qualitative dependence of the quality factor and photon flux absorptance of the two-port power combiner on the normalized capacitance modulation amplitude $\Delta C/C$ (ΔC

https://doi.org/10.1021/acsphotonics.1c00981
ACS Photonics 2021, 8, 3034−3041

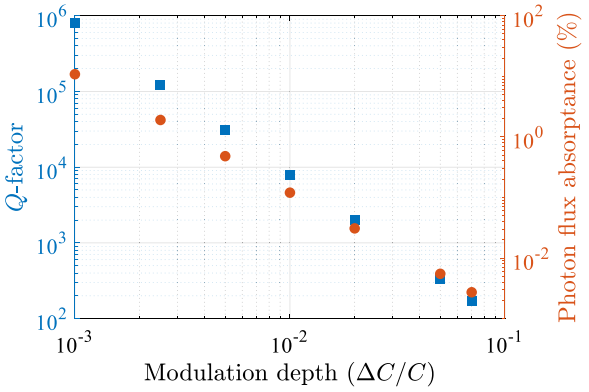

Figure 8. Dependence of the quality factor and photon flux absorptance of the two-port power combiner on the capacitance modulation depth. The space−time modulation function of the metasurface was optimized separately for each of the seven discrete values of $\Delta C/C$.

and C refer to the variation range and the average value of the capacitance, respectively). For this analysis, we introduce losses in the capacitive layer by modeling the capacitance as a complex number where the imaginary part represents losses (see section 6 of Supporting Information). In addition, we chose the permittivity of the substrate $\epsilon_r = 2.08(1 - j10^{-7})$ and its thickness $d/\lambda_0 = 0.1$. Such material parameters correspond to SiO_2 at the telecom frequency band and match those in the example considered below. The modulation frequency is selected as $\omega_M = 0.02\omega_0$.

For each of the seven discrete values of $\Delta C/C$, we optimized the space−time modulation function in (4) and achieved the maximal combining efficiency (with zero parasitic reflections and limited only by absorption in the substrate). As is seen from Figure 8, with increasing modulation depth, the quality factor of the combiner and photon absorption decrease dramatically. This is because for strong modulation depth, the required excited surface mode ($n = +2$ mode for incidence from port 2) becomes weak, in agreement with observations in previous studies about space−time systems.[15,17] Note that in Figure 8 we only show several discrete points of the modulation depth. In general, for any modulation depth between the studied discrete points, one can always find an optimal modulation function that provides power combining with high efficiency.

We also studied the effect of the modulation frequency ω_M on the device performance. We have found that the performance is rather robust with respect to different choices of the modulation frequency. For different ω_M in the range from $0.0002\omega_0$ to $0.02\omega_0$, it is always possible to find a space−time modulation function providing high efficiency without parasitic reflections (see section 7, Supporting Information), and the corresponding system quality factor does not change.

At microwave frequencies (ω_0 in the GHz range), the modulation of capacitance can be realized by discrete varactors. Typically, $\Delta C/C$ on the order of 0.1−1 can be obtained with the modulation frequency above 1 GHz.[28,34] Such implementations of different devices were reported in refs 16, 22, 24, 28, and 29. In Supporting Information (section 8), we show that by discretizing one spatial period into at least 10 subcells, the above calculated combining efficiency can be achieved. At infrared frequencies, the modulated capacitive metasurface sheet can be effectively realized with a homogeneous[35] or patterned material film[25,36] with a modulated permittivity. Implementation of combiner metasurfaces can be achieved using two previously reported approaches: based on electro-optic modulations of lithium niobate ($LiNBO_3$)[36] or a nonlinear Kerr effect in silicon.[25] Since both materials possess very small attenuation coefficients at near-infrared, the power dissipation in the metasurface can be neglected. Electro-optic modulations typically have a small modulation frequency on the order of $\omega_M = 2\pi \times 40$ GHz, which corresponds to $0.0002\omega_0$ at $\omega_0 = 2\pi \times 200$ THz ($\lambda_0 = 1.5$ μm).[32] The permittivity modulation amplitude in lithium niobate is relatively small ($\sim 10^{-3}$); however, the effect of electro-optic modulation can be enhanced by highly resonant patterning of the metasurface.[36]

In contrast, permittivity modulation based on the nonlinear Kerr effect can achieve a large modulation frequency of the order of $\omega_M = 0.02\omega_0 = 2\pi \times 4$ THz for $\lambda_0 = 1.5$ μm. In this approach, the modulation is generated by heterodyne interference between two pump laser beams that are closely spaced in frequency. While the permittivity modulation resulting from the nonlinear Kerr effect is small, relatively large modulation of the reflection coefficient phase was experimentally reported due to local field enhancement by metasurface resonant elements.[25] Using the results of ref 25, we have estimated that their silicon patterned layer has an effective capacitance with the modulation depth on the order of $\Delta C/C \approx 0.07$. Such a value suggests that the metasurface power combiner can be designed for operation at optical frequencies with a moderate quality factor $Q \approx 170$ and negligible photon flux absorptance (see Figure 8, which is plotted for the case with the same substrate properties). In addition, reducing the substrate thickness can further reduce the quality factor of the device.

CONCLUSION

In summary, we have introduced the concept of perfect power combining using space−time metasurfaces. Using proper traveling-wave modulation in the metasurface, arbitrary numbers of incident plane waves can be redirected toward one output port with nearly 100% efficiency. The presented method is general and can be applied from microwave to optical frequencies. Since the designed metasurface power combiner has a finite bandwidth, it is possible to extend the concept to complete and phase-independent combination of incident light pulses, provided that their spectra are within the device bandwidth. Perfect pulse combination is essential for obtaining high-intensity laser sources and has important applications for laser-plasma accelerators,[37,38] particle sources (e.g., ion),[39] secondary radiation generation,[40] and so on.

ASSOCIATED CONTENT

Supporting Information

The Supporting Information is available free of charge at https://pubs.acs.org/doi/10.1021/acsphotonics.1c00981.

Efficiency bound on power combining for multiport inputs. Efficiency bound of power coupling for single-port input. Mode-matching method. Scattering matrix of the three-port power combiner. Design of a four-port power combiner. Modeling lossy capacitive layer. Effect of the modulation frequency on power combining. Discretization of the modulation function (PDF)

https://doi.org/10.1021/acsphotonics.1c00981
ACS Photonics 2021, 8, 3034−3041

AUTHOR INFORMATION

Corresponding Author

Xuchen Wang − *Department of Electronics and Nanoengineering, Aalto University, FI-00076 Aalto, Finland;* orcid.org/0000-0002-5997-1130; Email: xuchen.wang@aalto.fi

Authors

Viktar S. Asadchy − *Ginzton Laboratory and Department of Electrical Engineering, Stanford University, Stanford, California 94305, United States;* orcid.org/0000-0002-9840-4737

Shanhui Fan − *Ginzton Laboratory and Department of Electrical Engineering, Stanford University, Stanford, California 94305, United States;* orcid.org/0000-0002-0081-9732

Sergei A. Tretyakov − *Department of Electronics and Nanoengineering, Aalto University, FI-00076 Aalto, Finland*

Complete contact information is available at: https://pubs.acs.org/10.1021/acsphotonics.1c00981

Notes

The authors declare no competing financial interest.

ACKNOWLEDGMENTS

This work was supported by the Academy of Finland (Project 330260) and the U.S. Air Force Office of Scientific Research MURI project (Grant No. FA9550-18-1-0379).

REFERENCES

(1) Pozar, D. M. *Microwave Engineering*; John Wiley & Sons, 2011.
(2) He, S.; Liu, K. On the possibility of a perfect power combiner. *Progress In Electromagnetics Research* **2017**, *158*, 1−6.
(3) Hanna, M.; Guichard, F.; Zaouter, Y.; Papadopoulos, D. N.; Druon, F.; Georges, P. Coherent combination of ultrafast fiber amplifiers. *J. Phys. B: At., Mol. Opt. Phys.* **2016**, *49*, 062004.
(4) Baranov, D. G.; Krasnok, A.; Shegai, T.; Alù, A.; Chong, Y. Coherent perfect absorbers: linear control of light with light. *Nature Reviews Materials* **2017**, *2*, 1−14.
(5) Uberna, R.; Bratcher, A.; Tiemann, B. G. Coherent polarization beam combination. *IEEE J. Quantum Electron.* **2010**, *46*, 1191−1196.
(6) Minott, P. O.; Abshire, J. B. Grating Rhomb Diode Laser Power Combiner. *Optical Technologies for Space Communication Systems*; Proc. SPIE *0756*; 3 June 1987; DOI: 10.1117/12.940022.
(7) Smits, F. Power Combiners for Incoherent Waves. Report Number *EUR-CEA-FC--1474*; IAEA: France, 1993; https://inis.iaea.org/search/search.aspx?orig_q=RN:24073780.
(8) Madasamy, P.; Jander, D. R.; Brooks, C. D.; Loftus, T. H.; Thomas, A. M.; Jones, P.; Honea, E. C. Dual-grating spectral beam combination of high-power fiber lasers. *IEEE J. Sel. Top. Quantum Electron.* **2009**, *15*, 337−343.
(9) Belousov, V.; Denisov, G.; Peskov, N. Y. Quasi-optical multiplexer based on reflecting diffraction grating. *Int. J. Infrared Millimeter Waves* **1991**, *12*, 1035−1043.
(10) Chann, B.; Huang, R.; Missaggia, L.; Harris, C.; Liau, Z.; Goyal, A.; Donnelly, J.; Fan, T.; Sanchez-Rubio, A.; Turner, G. Near-diffraction-limited diode laser arrays by wavelength beam combining. *Opt. Lett.* **2005**, *30*, 2104−2106.
(11) Thumm, M. K.; Kasparek, W. Passive high-power microwave components. *IEEE Trans. Plasma Sci.* **2002**, *30*, 755−786.
(12) Mirmoosa, M.; Ptitcyn, G.; Asadchy, V.; Tretyakov, S. Time-Varying Reactive Elements for Extreme Accumulation of Electromagnetic Energy. *Phys. Rev. Appl.* **2019**, *11*, 014024.
(13) Galiffi, E.; Wang, Y.-T.; Lim, Z.; Pendry, J.; Alù, A.; Huidobro, P. A. Wood anomalies and surface-wave excitation with a time grating. *Phys. Rev. Lett.* **2020**, *125*, 127403.
(14) Shaltout, A.; Kildishev, A.; Shalaev, V. Time-varying metasurfaces and Lorentz non-reciprocity. *Opt. Mater. Express* **2015**, *5*, 2459−2467.
(15) Wang, X.; Díaz-Rubio, A.; Li, H.; Tretyakov, S. A.; Alù, A. Theory and design of multifunctional space-time metasurfaces. *Phys. Rev. Appl.* **2020**, *13*, 044040.
(16) Cardin, A. E.; Silva, S. R.; Vardeny, S. R.; Padilla, W. J.; Saxena, A.; Taylor, A. J.; Kort-Kamp, W. J.; Chen, H.-T.; Dalvit, D. A.; Azad, A. K. Surface-wave-assisted nonreciprocity in spatio-temporally modulated metasurfaces. *Nat. Commun.* **2020**, *11*, 1−9.
(17) Hadad, Y.; Sounas, D.; Alù, A. Space-time gradient metasurfaces. *Phys. Rev. B* **2015**, *92*, 100304.
(18) Shi, Y.; Han, S.; Fan, S. Optical circulation and isolation based on indirect photonic transitions of guided resonance modes. *ACS Photonics* **2017**, *4*, 1639−1645.
(19) Taravati, S.; Kishk, A. A. Dynamic modulation yields one-way beam splitting. *Phys. Rev. B* **2019**, *99*, 075101.
(20) Asadchy, V.; Díaz-Rubio, A.; Tcvetkova, S.; Kwon, D.-H.; Elsakka, A.; Albooyeh, M.; Tretyakov, S. Flat engineered multichannel reflectors. *Phys. Rev. X* **2017**, *7*, 031046.
(21) Wang, X.; Díaz-Rubio, A.; Asadchy, V. S.; Ptitcyn, G.; Generalov, A. A.; Ala-Laurinaho, J.; Tretyakov, S. A. Extreme asymmetry in metasurfaces via evanescent fields engineering: Angular-asymmetric absorption. *Phys. Rev. Lett.* **2018**, *121*, 256802.
(22) Wu, Z.; Scarborough, C.; Grbic, A. Space-Time-Modulated Metasurfaces with Spatial Discretization: Free-Space N-Path Systems. *Phys. Rev. Appl.* **2020**, *14*, 064060.
(23) Li, A.; Li, Y.; Long, J.; Forati, E.; Du, Z.; Sievenpiper, D. Time-moduated nonreciprocal metasurface absorber for surface waves. *Opt. Lett.* **2020**, *45*, 1212−1215.
(24) Lira, H.; Yu, Z.; Fan, S.; Lipson, M. Electrically driven nonreciprocity induced by interband photonic transition on a silicon chip. *Phys. Rev. Lett.* **2012**, *109*, 033901.
(25) Guo, X.; Ding, Y.; Duan, Y.; Ni, X. Nonreciprocal metasurface with space−time phase modulation. *Light: Sci. Appl.* **2019**, *8*, 1−9.
(26) Oue, D.; Ding, K.; Pendry, J. B. Calculating spatiotemporally modulated surfaces: A dynamical differential formalism. *Phys. Rev. A* **2021**, *104*, 013509.
(27) Collin, R. E. *Foundations for Microwave Engineering*; John Wiley & Sons, 2007; pp 804−807.
(28) Taravati, S.; Chamanara, N.; Caloz, C. Nonreciprocal electromagnetic scattering from a periodically space-time modulated slab and application to a quasisonic isolator. *Phys. Rev. B* **2017**, *96*, 165144.
(29) Hadad, Y.; Soric, J. C.; Alù, A. Breaking temporal symmetries for emission and absorption. *Proc. Natl. Acad. Sci. U. S. A.* **2016**, *113*, 3471−3475.
(30) Correas-Serrano, D.; Alù, A.; Gomez-Diaz, J. S. Magnetic-free nonreciprocal photonic platform based on time-modulated graphene capacitors. *Phys. Rev. B* **2018**, *98*, 165428.
(31) Wang, J.; Herrmann, J. F.; Witmer, J. D.; Safavi-Naeini, A. H.; Fan, S. Photonic modal circulator using temporal refractive-index modulation with spatial inversion symmetry. *Phys. Rev. Lett.* **2021**, *126* DOI: 10.1103/PhysRevLett.126.193901
(32) Williamson, I. A.; Minkov, M.; Dutt, A.; Wang, J.; Song, A. Y.; Fan, S. Integrated Nonreciprocal Photonic Devices With Dynamic Modulation. *Proc. IEEE* **2020**, *108*, 1759−1784.
(33) Zhou, T.; Sano, T.; Wilcox, R. Coherent combination of ultrashort pulse beams using two diffractive optics. *Opt. Lett.* **2017**, *42*, 4422−4425.
(34) Taravati, S.; Eleftheriades, G. V. Pure and Linear Frequency-Conversion Temporal Metasurface. *Phys. Rev. Appl.* **2021**, *15*, 064011.
(35) Tretyakov, S. *Analytical Modeling in Applied Electromagnetics*; Artech House, 2003; pp 38−41.
(36) Barton, D., III; Lawrence, M.; Dionne, J. Wavefront shaping and modulation with resonant electro-optic phase gradient metasurfaces. *Appl. Phys. Lett.* **2021**, *118*, 071104.
(37) Leemans, W.; Esarey, E. Laser-driven plasma-wave electron accelerators. *Phys. Today* **2009**, *62*, 44−49.

(38) Esarey, E.; Schroeder, C.; Leemans, W. Physics of laser-driven plasma-based electron accelerators. *Rev. Mod. Phys.* **2009**, *81*, 1229.
(39) Haseroth, H.; Hora, H. Physical mechanisms leading to high currents of highly charged ions in laser-driven ion sources. *Laser Part. Beams* **1996**, *14*, 393−438.
(40) Daido, H.; Nishiuchi, M.; Pirozhkov, A. S. Review of laser-driven ion sources and their applications. *Rep. Prog. Phys.* **2012**, *75*, 056401.

https://doi.org/10.1021/acsphotonics.1c00981
ACS Photonics 2021, 8, 3034−3041